

Multiple Modes of Motion for the Effectiveness of Outer Hair Cells at High Frequencies

Kuni H. Iwasa

NIDCD, National Institutes of Health
Bethesda, MD 20892, USA

version: 15 April 2024

Abstract

Outer hair cells (OHCs) are essential for the sensitivity and frequency specificity of the mammalian ear. To perform this function, OHCs need to amplify the motion of the basilar membrane (BM), which is much stiffer than themselves. If OHCs and the BM are components of a single oscillator, this impedance mismatch seriously limits the effectiveness of OHCs. However, the elaborated structure of the organ of Corti can support multiple modes of motion. Here, systems of two coupled oscillators are examined as the simplest models of the system with multiple modes of motion. It is found that some of these model systems have conditions, under which an OHC can function as an effective amplifier, overcoming the impedance mismatch. The present examination suggests that the presence of multiple modes of motion is a key to the exquisite performance of the mammalian ear.

Introduction

The mammalian hearing range may extend up to 100 kHz or beyond [1], depending on the species, quite remarkable for a biological system. Such function may call for a special rapid mechanism. Indeed, it is shown that the motility of outer hair cells (OHCs) based on “electromotility,” a kind of piezoelectricity, with which their cylindrical cell bodies are driven by the receptor potential, is essential for the sensitivity and frequency selectivity of the mammalian ear [2]. In addition, how OHCs are integrated into the rest of the cochlea is a critical issue, which requires extensive study to understand the mechanical basis of the mammalian hearing [3, 4].

Some of the earlier theories treated the activity of OHCs as an additional pressure applied to the basilar membrane [5] or impedance of the basilar membrane [6, 7]. Some other treatments placed OHCs between two inertial masses,

resulting in multiple degrees of freedom [8–11]. The goal of these theories has been to explain the tuning curve of the ear.

Now, let us focus on the issue of the upper bound of auditory frequency. One of the difficulties of explaining the effectiveness of OHCs was the low-pass nature of their intrinsic electric circuit. This problem can be addressed by introducing piezoelectric resonance [12, 13]. However, the model employed in the treatment assumed that soft OHCs and the stiff basilar membrane (BM) are components of the same oscillator. The upper limit obtained was ~ 10 kHz, much higher than the roll-off frequency (up to several kHz) of the intrinsic electric circuit, but still not high enough for covering the auditory frequency [13].

A possible solution to this problem is that the OHCs and the basilar membrane are elements of separate oscillators, and those oscillators are coupled so that energy can be transferred between them. Multiple modes of motion appears to be consistent with recent experimental reports, including those with optical coherence tomography (OCT) [14]. Those reports show complex motion of the inner ear, which depends on the stimulation intensity as well as frequency [15–18].

Here we examine a set of two oscillators, heavy and light, coupled with either elastic or viscous element as the simplest examples of a system with multiple modes of motion. As a control, a single mode oscillator with an OHC is described to illustrate the effect of impedance mismatch. Then systems of two coupled oscillators are examined. The light oscillator (LO) incorporates an OHC and the heavy one (HO) includes the basilar membrane. Coupling is either elastic or viscous. The OHC is stimulated by either the motion of HO or that of LO.

The present treatment focuses on local energy balance, and intended to address the upper bound of the auditory frequency. Such a location may correspond to the basal end of the cochlea, where traveling waves start.

Single mode of motion

Let us start from a simple model oscillator system, in which an OHC incorporated as illustrated in Fig. 1. Here we follow the one-dimensional model [13], rather than the more realistic cylindrical model [19] for simplicity.

First, we drive the system by an external force F . The equation of motion can be written down as

$$\left(m \frac{d^2}{dt^2} + \eta \frac{d}{dt} + k_e\right) X = k_o(X_\infty - X) + F, \quad (1)$$

where m is the mass, η drag coefficient, k_e the stiffness of the external elastic load, k_o the material stiffness of the OHC, X is the length of the OHC, and k_e the stiffness of external load. X_∞ is the length of the cell, which satisfies the equilibrium condition for the voltage V at the given moment.

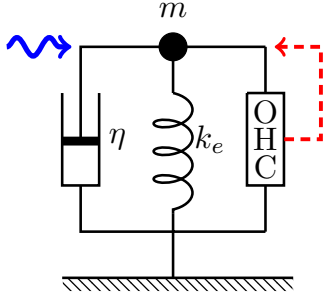


Figure 1: A single oscillator with an OHC. The oscillator consists of mass m , an external elastic element with stiffness k_e , and a damper with drag coefficient η and an outer hair cell (OHC), which responds to the movement of mass (dashed red arrow). This system is driven by a sinusoidal waveform with angular frequency ω (wavy blue arrow).

If the force applied is a periodic waveform with angular frequency ω , we can write

$$V = V_0 + v \exp[i\omega t], \quad (2a)$$

$$X = X_0 + x \exp[i\omega t], \quad (2b)$$

$$F = F_0 + f \exp[i\omega t], \quad (2c)$$

where V is the receptor potential, which is generated by the mechanosensitivity of the hair bundle.

Then we have

$$x \left(-\bar{\omega}^2 + i \frac{\bar{\omega}}{\bar{\omega}_\eta} + 1 + \frac{k u_a}{k_e + k_o} \right) = -\frac{k_o}{k_e + k_o} u_b v + \frac{f}{k_e + k_o}, \quad (3)$$

where $\bar{\omega} (= \omega/\omega_r)$ is the frequency normalized to the mechanical resonance frequency $\omega_r = \sqrt{(k_e + k_o)/m}$, and $\bar{\omega}_\eta$ is normalized viscoelastic roll-off frequency. Parameters u_a and u_b depend on the piezoelectric properties of the OHC (See Table 1). For derivation, see Appendix A.

Now, consider that the voltage waveform is generated by changes of hair bundle resistance \hat{r} due to bending. The effect of hair bundle resistance R_a on the membrane potential V can be expressed

$$(e_{ec} - V)/R_a = (V - e_K)/R_m + C_0 dV/dt - Nq dP/dt, \quad (4)$$

where e_{ec} is the endocochlear potential, e_K is the resting potential of OHC, which is primarily determined by K^+ conductance, R_a hair bundle conductance, C_0 the voltage-independent membrane capacitance of the cell, q and N , respectively, the unit charge the motile element transfers across the membrane and the number of such motile elements in the cell. P is the fraction of such motile elements in the extended state, which contributes to elongation of the cylindrical cell.

With periodic stimulation, the hair bundle conductance R_a consists of a time independent component R_0 and a sinusoidal component with relative amplitude \hat{r} . Thus the receptor current with frequency ω is expressed by

$$-i_0 \hat{r} = (\sigma + i\omega C_0)v - i\omega Nqp. \quad (5)$$

Here $i_0 = (e_{ec} - e_K)/(R_0 + R_m)$ is the steady state current and $\sigma = 1/R_0 + 1/R_m$ the steady state conductance, which can be dropped for high frequency stimulation because it is smaller than ωC_0 . The quantity p is the amplitude of P with frequency ω .

Thus the variable v can be replaced by \hat{r} ,

$$(-\bar{\omega}^2 + i\bar{\omega}/\bar{\omega}_\eta + 1 + \gamma B)x = i\frac{\gamma A}{\bar{\omega}} \hat{r} + \hat{f}, \quad (6)$$

where

$$A = \frac{uk_o}{\omega_r(k_e + k_o)} \quad (7a)$$

$$B = u_a k / (k_e + k_o) + u_q, \quad (7b)$$

$$\hat{f} = f / (k_e + k_o). \quad (7c)$$

Here u , u_a , and u_q are quantities that represent hair bundle sensitivity and piezoelectricity. See Table 1 for definitions (for derivations see Appendix A). The quantity γ represents relative voltage sensitivity of prestin, the motile membrane protein of OHCs [20]. The maximal value is set to unity (i.e. $0 \leq \gamma \leq 1$). It will be referred to as the “operating point parameter.” Notice also that both A and B depend on the ratio k_e/k_o of external load to the intrinsic stiffness of the OHC.

The first term of the right-hand side of Eq. 6, which contains A , works as an amplifying term, counteracting the drag term on the left-hand side. However, it is inversely proportional to the frequency ω , unlike negative drag. The reason for this frequency dependence stems from the receptor potential (Eq. 5), where capacitive current overwhelms resistive current at high frequencies. The parameter B represents the contribution of the motile element to the stiffness of the cell body of the OHC.

For a small amplitude x , \hat{r} can be proportional to x . Thus, we may put $\hat{r} = gx$. This substitution leads to the equation of motion for the single mode model

$$[-\bar{\omega}^2 + i(\bar{\omega}/\bar{\omega}_\eta - \gamma g A/\bar{\omega}) + 1 + \gamma B]x = \hat{f}. \quad (8)$$

Notice the amplitude x increases by the term with A , which counteracts the drag term.

The performance of the OHC in the system can be quantified by power gain $G(\omega)$, which is the ratio of power output to power input. Power output is in the form of viscous dissipation $\eta |dX/dt|^2$ because other the component is recovered during a cycle. Power input can be expressed as $\text{Re}[F \cdot dX/dt]$. Thus, this quantity can be expressed by

$$\begin{aligned} G(\omega) &= \eta \omega^2 |x|^2 / |\omega f \text{Im}[x]| \\ &= \eta \omega |x| / (f \sin \phi), \end{aligned} \quad (9)$$

Table 1: Parameter definitions. k_B Boltzmann’s constant, T the temperature. * The motile function of OHCs is described by a two state model. P_0 is the fraction of one of the two states in a single cell at the operating point. ** The definition of κ given here assumes the presence of k_c , the elastic element between the two oscillators. In the absence of such coupling, $k_c = 0$. See Appendix A for derivations.

symbol	definition	parameter	definition
P_0	motor conformation*	γ	$4P_0(1 - P_0)$
β	$1/(k_B T)$	u_a	$\beta a^2 k_o N/4$
a	prestin displacement	u_b	$\beta a q N/4$
q	prestin charge	u	$\beta i_0 a q N/(4C_0)$
N	number of prestin	u_q	$\beta q^2 N/(4C_0)$
C_0	cell capacitance	κ **	$k_o/(k_o + k_e + k_c)$
i_0	resting current	ω_r	resonance frequency
k_o	cell stiffness	A	$(u/\omega_r) \kappa$
k_e	parallel elastic load	B	$u_a(1 - \kappa) + u_q$

where x is given by Eq. 8, $\text{Re}[\dots]$ and $\text{Im}[\dots]$ represent, respectively, real part and imaginary part, and ϕ is the absolute value of the phase angle of x with respect to external force. In the absence of the OHC, i.e. $A = B = 0$, we obtain $G(\omega) = 1$ as expected.

Even though we have assumed that the amplitude x is small, Eq. 8 may leads to a large x , depending on the parameter values. In such cases, such an amplitude should be an artifact of linearization. The main reason is that the coefficient g must be smaller for a large x due to nonlinearity of the response function. In addition, the factors A and B are also affected because they depend on γ , which is determined by the operating point of electromotility.

Coupled oscillator models

Consider a system with two harmonic oscillators, light and heavy. The light oscillator (LO) consists of an OHC and an elastic load k_e and inertia m . The displacement of this oscillator is X . The heavy oscillator (HO) consists of the basilar membrane and inertia M , an elastic element with stiffness K , and viscous load with drag coefficient η . We can assume in general that the two oscillators are coupled by an elastic element with stiffness k_c and a viscous element with drag coefficient η_c , and external force F is applied to the HO.

The motion of the two oscillators are described by,

$$\left(m \frac{d^2}{dt^2} + \eta_1 \frac{d}{dt} + k_e + k_o + \gamma B\right) X = i \frac{\gamma A}{\omega} \hat{r} + \left(k_c + \eta_c \frac{d}{dt}\right) (Y - X) \quad (10a)$$

$$\left(M \frac{d^2}{dt^2} + \eta_2 \frac{d}{dt} + K\right) Y = \left(k_c + \eta_c \frac{d}{dt}\right) (X - Y) + F(t), \quad (10b)$$

where quantities A and B are defined by Eq. 7 with viscous coupling but elastic load modifies these quantities. That means

$$A = (u/\omega_r) k_0 / (k_e + k_o + k_c) \quad (11a)$$

$$B = u_a (k_e + k_c) / (k_e + k_c + k_o) + u_q. \quad (11b)$$

For this reason, the quantities A and B depends on k_c even in the case where k_e is kept constant.

An issue for this model is which oscillator include the presence of the main drag with coefficient η . Here we assume that the main drag belongs to HO because the HO is heavier than the LO. In the case we assume that the main drag belong to LO, it turns out that the OHC only amplifies the amplitude of LO and it cannot affect the oscillation of HO.

OHC works on the LO, its hair bundle sensing the displacement X of LO or the displacement Y of the HO, or both. For simplicity, let us consider only two cases, introducing the hair bundle sensitivity g to displacements: $\hat{r} = gX$, where the hair bundle senses the displacement of LO, and $\hat{r} = gY$ where the hair bundle senses the displacement of HO.

Classical analyses show that energy transfer between two coupled oscillators is rather complex despite the apparent simplicity of the equations [21, 22]. For simplicity, here we only examine only the response to continuous sinusoidal stimulation and separate each displacement into a constant component and time dependent component.

$$F = F_0 + f_B \exp[i\omega t], \quad (12a)$$

$$X = X_0 + x \exp[i\omega t], \quad (12b)$$

$$Y = Y_0 + y \exp[i\omega t], \quad (12c)$$

where ω is the angular frequency of stimulation.

Power gain $G(\omega)$ is obtained analogous to Eq. 9 for the simple oscillator,

$$G(\omega) = \eta\omega|y| / (f_B \sin \varphi), \quad (13)$$

where φ is the absolute value of the phase angle of y . Notice that amplifier gain here is determined by the amplitude y of HO because both external force and drag work on HO.

In general, bending of the OHC hair bundle may depend on x , the displacement of the LO as well as y , the displacement of the HO. The simplest

assumption to represent such dependence would be to express \hat{r} as a linear combination of x and y . For simplicity, two extreme cases will be examined at first: the case where \hat{r} depends only on y , and another where it depends only on x . Then we proceed to a more general case, where \hat{r} depends on the combination of x and y .

Since we have so many parameters, we reduce the number of parameters by considering a number of separate cases. First, coupling includes viscous and elastic components. However, we assume coupling is purely elastic or purely viscous. Second, we further assume that the hair bundle of the OHC is stimulated either by the displacement of the HO, which incorporates the basilar membrane, or the displacement of the LO, which includes the OHC. For brevity, let us call the former as ‘‘HO-driven mode’’ and the latter ‘‘LO-driven mode.’’

If we assume that subreticular drag is the dominant one, the drag coefficient of which is η , the HO-driven case includes the subreticular drag because both depend on displacement y . Thus, $\eta_2 = \eta$ and $\eta_1 = 0$. In LO-driven mode, likewise $\eta_2 = 0$ and $\eta_1 = \eta$ because they are both associated with x , the displacement of the LO.

HO-driven case

We assume that the main drag of the system belongs to HO, and that the dominant drag is due to the shearing motion in the subreticular space, then a natural assumption would be that the hair bundle of the OHC is stimulated by the motion of the HO. Then, we may express changes of the hair bundle conductance by $\hat{r} = gY$ with the sensitivity g .

Viscous coupling

Let us start from the system with viscous coupling with characteristic frequency ω_η on the heavy oscillator. Given the stiffness ratio s of the heavy oscillator to the light oscillator, the characteristic frequency on the light oscillator is ω_η/s . Introducing new parameters defined by $f = f_B/K$ and $s = K/k$, the set of equations can be written as

$$[-(\bar{\omega}/\bar{\omega}_1)^2 + 1 + is\bar{\omega}/\bar{\omega}_c + \gamma B]x - i[\gamma Ag/\bar{\omega} + s\bar{\omega}/\bar{\omega}_c]y = 0, \quad (14a)$$

$$-i\bar{\omega}/\bar{\omega}_c x + [-\bar{\omega}^2 + i\bar{\omega}/\bar{\omega}_\eta + 1 + i\bar{\omega}/\bar{\omega}_c]y = f, \quad (14b)$$

where ω_r is the resonance angular frequency of the HO, i.e. $\omega_r^2 = K/M$ and the frequency is normalized to this resonance frequency. For example $\bar{\omega} = \omega/\omega_r$ and $\bar{\omega}_c = \omega_c/\omega_r$ with $\omega_c = K/\eta_c$. The quantity $\bar{\omega}_1$ is the ratio of the resonance frequency of the LO to that of HO. Notice that f has the dimensionality of length.

Elastic coupling

Elastic coupling introduces an elastic element K_c in each of the equation of motion, elevating the resonance frequency more significantly in LO than in

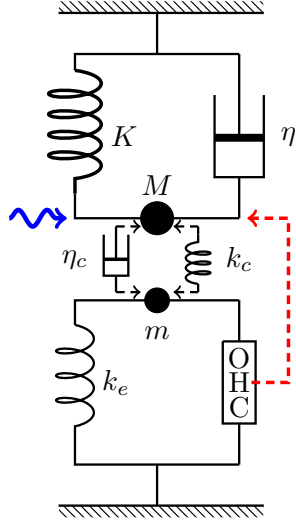


Figure 2: Coupled oscillators, in which OHC is driven by the HO. The HO (top) consists of mass M , an elastic element with stiffness K , and a damper with drag coefficient η . The light oscillator (bottom) consists of mass m , an elastic element with stiffness k_e an OHC, which responds to the movement of the HO (dashed red arrow). The HO is driven by a sinusoidal waveform with angular frequency ω (wavy blue arrow) and the two oscillators are coupled either by an elastic element with stiffness k_c or by a damper with viscous coefficient η_c .

HO. Since energy transfer between the oscillators depends on the difference in the resonance frequencies of the two oscillators, adjustment should be made to minimize the difference in the resonance frequency.

$$[-(\bar{\omega}/\bar{\omega}_1)^2 + 1 + cs + \gamma B]x - [i\gamma Ag/\bar{\omega} + cs]y = 0, \quad (15a)$$

$$-cx + [-\bar{\omega}^2 + i\bar{\omega}/\bar{\omega}_\eta + 1 + c]y = f, \quad (15b)$$

introducing new parameters c and $\bar{\omega}_1$. Of these parameters, c is defined by $c = k_c/K$. We may assume $c < 1$ because the coupling should not be too strong.

The parameter $\bar{\omega}_1$ is to eliminate the dependence of the resonance frequency of LO by the elastic coupling element, which elevates the resonance frequency. This effect is less significant for the HO because c is small. However, it is quite pronounced for the LO if the ratio s is large. This effect should be compensated because a larger difference in the resonance frequencies of the two oscillators decreases energy transfer between the oscillators. The parameter $\bar{\omega}_1$, in effect, allows adjustment of the mass of the LO so that energy transfer is optimized for a large values for the ratio s .

LO-driven case

An alternative assumption regarding OHC stimulation is that the displacement x of the LO affects the bending of OHC hair bundle, creating a direct feedback loop.

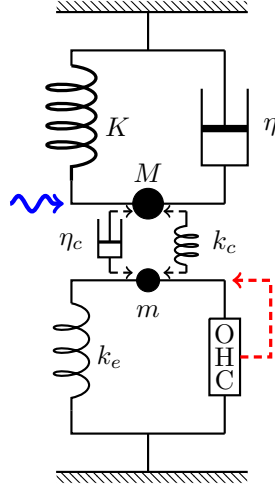


Figure 3: LO-driven coupled oscillators. The HO consists of mass M , an elastic element with stiffness K , and a damper with drag coefficient η . The LO (bottom) consists of mass m , an elastic element with stiffness k_e , an OHC, which responds to the movement of the LO (dashed red arrow). The HO is driven by a sinusoidal waveform with angular frequency ω (wavy blue arrow) and the two oscillators are coupled either by an elastic element with stiffness k_c or a dashpot with viscous coefficient η_c .

Viscous coupling

The set of equations of motion can be written as

$$[-(\bar{\omega}/\bar{\omega}_1)^2 - i\gamma Ag/\bar{\omega} + 1 + is\bar{\omega}/\bar{\omega}_c + \gamma B]x - is\bar{\omega}/\bar{\omega}_c y = 0, \quad (16a)$$

$$-i\bar{\omega}/\bar{\omega}_c x + [-\bar{\omega}^2 + i\bar{\omega}/\bar{\omega}_\eta + 1 + i\bar{\omega}/\bar{\omega}_c]y = f. \quad (16b)$$

The phase relationship between x and y is determined by Eq. 16a.

Elastic coupling

The time dependent components follow the following equation

$$[-(\bar{\omega}/\bar{\omega}_1)^2 + 1 + cs + \gamma B - i\gamma Ag/\bar{\omega}]x - csy = 0, \quad (17a)$$

$$-cx + [-\bar{\omega}^2 + i\bar{\omega}/\bar{\omega}_\eta + 1 + c]y = f, \quad (17b)$$

Eq. 17 indicates that the LO reduces, rather than increases, the amplitude of the HO if the effect of OHC is large. If the term $Ag/\bar{\omega}$ dominates over cs , Eq. 15a makes the phase of x delayed from that of y up to $-\pi/2$. In addition, the magnitude of x is expected to be larger near the resonance frequency ($\bar{\omega} \approx 1$) because the coefficient of x in Eq. 15a can be much smaller than the coefficient of y . This feature will be illustrated later with numerical examination.

General cases

OHCs can be stimulated by a combination of the displacement of LO and that of HO. In addition, the coupling of these two oscillators includes both viscous and elastic elements. Such cases are not examined here because those combinations introduce additional parameters, which are needed to describe relative significance of these terms.

Parameter values

Given the number of parameters in our set of equations, our numerical analysis is to survey conditions, under which the OHC is more effective in coupled oscillators than in the single mode oscillator as the amplifier.

In the following, values for A and B , which represent the activity of OHCs are examined using experimental data available in a best frequency range. Then the amplitude of the single mode model is evaluated. After that, the amplitudes of coupled oscillator models are evaluated. Finally, the effectiveness of the coupled oscillator models in higher frequency ranges will be discussed as an extrapolation.

For examining the performance of coupled oscillator models, experimental values obtained from guinea pigs near 20 kHz location are available. See Table 2.

Cellular factors (20 kHz)

Parameters A and B in the equations depend on the electromotility parameters u , u_a , and u_q (See Table 1). For a 20 μm long cell, typical of the 10 to 20 kHz cochlear region, the linear capacitance is $C_0 = 8$ pF and $an = 1\mu\text{m}$, which is 5% of the resting cell length. Most in vitro experiments show the unitary motile charge of $q = 0.8e$, where e is the electronic charge. The membrane potential is near the optimal range for the motile element. The resting basolateral resistance is 7 M Ω and the resting membrane potential of -50 mV requires the resting apical resistance of 30 M Ω . These values lead to $i_0 = 4$ nA. These parameter values are summarized in Table 2

Table 2: Parameter values at 20 kHz location

parameter	definition	value	source
C_0	structural capacitance of OHC	8 pF	
k_o	structural stiffness of OHC	20 mN/m	[23]
k_e	elastic load on OHC	adjustable	
K	BM stiffness per OHC	200/3 mN/m	see text
s_o	ratio K/k_o	10	
s	stiffness ratio K/k	~ 5	
i_0	mechanoreceptor current	4 nA	[24]
ω_η/ω_r	viscous roll-off frequency	12.5	see text
g	hair bundle sensitivity	1/(25 nm)	[25, 26]

The stiffness k_o of a 20 μm long OHC, which may correspond to the same location, is about 20 mN/m, given the specific stiffness of 510 nN/m per unit strain for guinea pigs [23]. However, this value may have some uncertainty.

The bottom part, up to 10 μm , of the OHC is held by the Deiters' cup. If this structure works as a damper [27], the length of elastic displacement is larger because the displacement includes the part within the cup. If, on the contrary, the structure is tight and rigid, not allowing slippage, the value of k_o must be higher.

The parameter values in Table 2 lead to a set of values for an OHC at 20kHz location:

$$u/\omega_r(20k) = 1.8, \quad u_a(20k) = 0.08, \quad u_q(20k) = 2. \quad (18)$$

Since $A = (u/\omega_r)\kappa$ and $B = u_a(1 - \kappa) + u_q$ as defined earlier by Eq. 7, B is approximately 2. It is not sensitive to the load ratio κ because it u_a is smaller than u_q .

Cochlear factors (20 kHz)

Let us assume that the characteristic stiffness of HO is that of the basilar membrane (BM). At the location of 20 kHz best frequency in guinea pigs is 3 mm from the stapes according to the Greenwood function, assuming the length of the BM is 18.5 mm [28, 29]. The stiffness of the location is about 0.21 N/m measured with a probe with 25 μm diameter tip [30]. This value is compatible with the ones obtained with a probe with 10 μm tip [31]. Thus, the stiffness ratio s_o is ~ 10 .

The intrinsic mechanical resonance frequency of the location is somewhat uncertain because of the so-called ‘‘half-octave shift’’ [3]. If the intrinsic mechanical resonance corresponds to the ‘‘passive’’ condition, the resonance frequency of the 20 kHz location is 14 kHz ($\omega_r = 20/\sqrt{2}$) being a half octave lower. However, it could be the opposite because viscous damping brings the peak to a lower frequency if it is not counteracted.

A significant contribution to friction is expected from the gap between the tectorial membrane and the reticular lamina. The friction coefficient of this gap can be estimated by a formula $\mu S^2/d$, where μ is the viscosity of the fluid, S the area of the gap per OHC, and d the gap, provided that the thickness of the boundary layer, which is $\sim 3.6 \mu\text{m}$ for 20 kHz [32], is greater than the gap. If we assume S is $10\mu\text{m} \times 15\mu\text{m}$ and d $1\mu\text{m}$, the friction coefficient is 1.2×10^{-7} N/m [13, 33]. With the resonance frequency of 14 kHz, the gap friction leads to a value 12.5 for ω_η/ω_r .

Extrapolation to higher frequencies

Extrapolation to higher frequencies includes OHC parameters, the amplification parameter A and the shift parameter B as well as the stiffness ratio s , which depends on the stiffness of the BM.

Of OHC parameters, B does not depend heavily on the resonance frequency because it is dominated by the electrical term u_q (See Eq. 7b). The amplification parameter A decreases at higher frequency locations because it is inversely

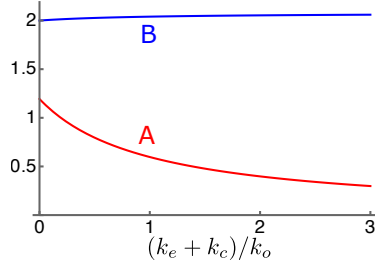


Figure 4: Dependence of parameters A (red) and B (blue) on the elastic load. The abscissa is $(k_e + k_c)/k_o$, the ratio of the external elastic load to the intrinsic stiffness of OHC.

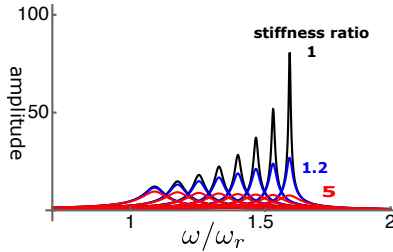


Figure 5: Amplitude of single mode oscillator plotted against frequency (normalized to ω_r). Stiffness ratio of load to OHC is 1, 1.2, and 5. γ (operating point variable) runs from 0.03 (left) to 0.24 with 0.03 increment. The unit of the ordinate axis is $f(= F/K)$.

proportional to the resonance frequency ω_r . However, such reduction is compensated by other factors. OHCs at higher frequency locations have larger resting current i_0 owing to larger hair bundle conductance and larger structural stiffness k_o of the cell body owing to its shorter cell length (See Eq. 7a and Table 1).

At higher frequency locations, the stiffness ratio s is expected to increase because the stiffness of the BM would increase more than the stiffness of OHCs. However, we proceed by assuming that the ratio s remains the same. The reason is an uncertainty in the effective length of OHCs. The stiffness is inversely proportional to the effective length of the lateral membrane, which is harder to determine with shorter OHCs because the connectivity in Deiters' cup is ambiguous as described earlier. In addition, somewhat higher values for s do not lead to qualitatively different results.

To examine high frequency performance aiming at 40kHz, twice higher than 20kHz, where parameter values are examined above, a numerical analysis is performed, assuming the following set of parameter vales:

$$u/\omega_r(40k) = 1.8/2, \quad B(40k) = 2, \quad k/k_o = 1, \quad s = 5, \quad \omega_\eta/\omega_r = 10. \quad (19)$$

It is expected that the frequency of the location is somewhat higher than 40 kHz.

Single mode oscillator

Let us start from the performance of the single mode oscillator before examining coupled oscillator models. The steady state amplitude is obtained by solving Eq. 8. The amplitude is normalized by the input \hat{f} (Figs. 5. As γ , the operating point variable of the OHC, increases, the peak amplitude shifts to

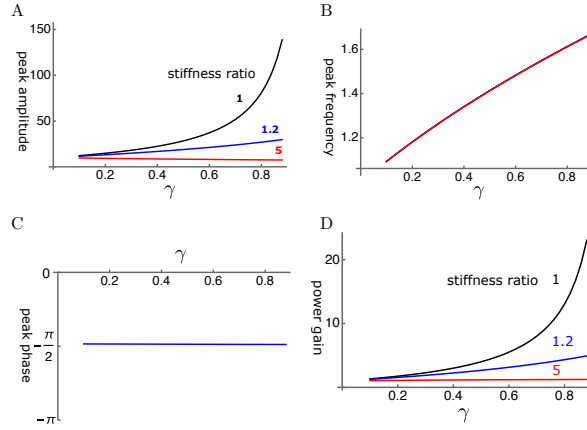


Figure 6: A: Peak amplitude, B: Peak frequency (normalized to the resonance frequency), C: peak phase, and D: The ratio of power output to power input are respectively plotted against γ , the operating point variable. The peak phase is $\pi/2$ in all cases.

higher frequencies independent of the elastic load (Fig. 6B)). The peak height sharply increases with γ if the elastic load is relatively small, i.e. the ratio k_e/k_o is 1 or smaller (Fig. 6A). However, the amplitude does not increase with γ even if k_e/k_o is as small as 1.2. With larger elastic load, such as $k_e/k_o \geq 5$, the peak amplitude does not increase at all.

The phase of the oscillator is delayed by $\pi/2$ as expected from the maximal amplitude of the damped oscillator (Fig. 6C). That makes the ratio of power output to power input similar to the amplitude of oscillation (Fig. 6D) because the power input insensitive to the magnitude of the drag. Thus, power gain is significantly attenuated by input impedance mismatch.

Coupled oscillators

In the following, we will examine if OHCs can be effective as amplifiers in coupled oscillators more than in a single mode oscillator. The coupled oscillator models have more parameters, which include stiffness ratio s and resonance frequency ratio ω_1 of the two oscillators, and coupling parameters (elastic element c and viscous element η_c).

Introduction of elastic coupling introduces an additional elastic load to the OHC. This affects A as well as B , which is not as sensitive as A . It also shifts the resonance frequency. Because this shift is much larger for LO, the resonance frequency of LO needs adjustment.

In the following, conditions for large gain in amplitude are sought in all four cases. Those cases are, HO driven modes with elastic coupling and viscous coupling, and LO driven modes with elastic and viscous coupling. For each condition, a single example is given. These examples are typical ones but they do not necessarily show all shared features of the conditions.

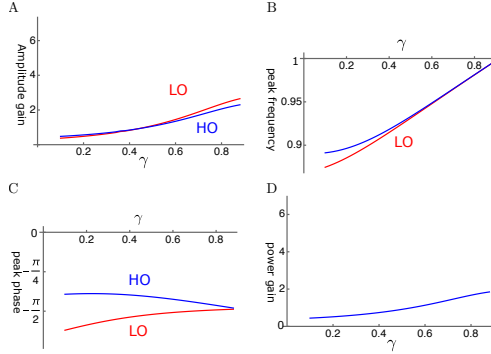


Figure 7: HO-driven viscosity coupled oscillators (HOV). A: Amplitude gain over SO mode, B: Peak frequency, and C: Peak phase with respect to the external force of each oscillator are plotted against γ , the operating point variable. LO (red) and HO (blue). D: Power input output ratio, which is closely related to HO. The set of parameter values: $1/\bar{\omega}_c=0.3$, $\omega_1=0.33$ in Eq. 14.

HO-driven cases

It would be natural to start from HO-driven mode because we assumed that HO is associated with the dominant drag, which likely stems from the shear in the subreticular space and this shear should stimulate the hair bundle of the OHC.

Viscous coupling

The Deiters' cup that links an OHC with the BM via Deiters' cell could provide viscous coupling due to its morphology. For this reason, it is of interest to examine the effect of viscous coupling.

Even though viscous coupling of the oscillators can have amplifying effect, it does not appear to be so effective. Amplitude gain tends to be much smaller than that of elastic coupling (Fig. 7A). Peak frequency of LO and that of HO are close to each other except for at small γ (Fig. 7B). The phase of HO is ahead of LO (Fig. 7C). Since the force LO applies to HO is by $\pi/2$ ahead of the phase of LO, LO amplifies the motion of HO. The ratio of power output to input ratio is rather small (Fig. 7D) as expected from the amplitude of HO.

Elastic coupling

Here, we assume that the coupling of the two oscillators is elastic. It is possible to find conditions, under which the amplitude of the LO reaches ~ 20 fold larger than the amplitude of the single mode oscillator (Fig. 8A). Here the abscissa is the operating point variable, which depends the voltage. It reaches unity at the optimal operating voltage. The amplitude of HO is about a half of that of LO. The peak frequency is about the same for the two oscillators and increases with the operating point variable (Fig. 8B).

The phase advance LO with respect to HO is consistent with the amplifying role of LO. However, the phase difference is rather small (Fig. 8C). The ratio of power output to power input coincides with the amplitude maximum of HO and reached about 6 at the peak (Fig. 8D).

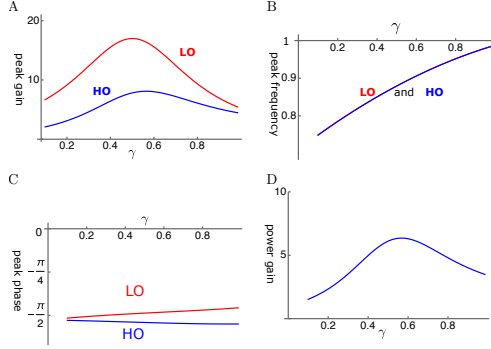


Figure 8: HO-driven elasticity coupled oscillators (HOE). A: Amplitude gain over SO mode, B: Peak frequency, and C: The phase with respect to the external force, of each oscillator are plotted against γ . LO (red) and HO (blue). D: The ratio of power output to power input. The set of parameter values: $c=0.2$, $\omega_1=0.29$ in Eq. 15.

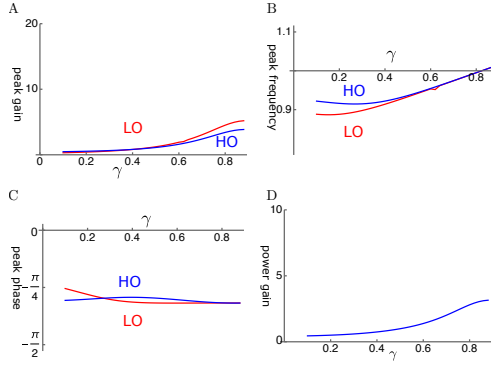


Figure 9: LO-driven viscosity-coupled oscillator (LOE). A: Amplitude gain over SO mode, B: Peak frequency, and C: The phase with respect to the external force, of each oscillator are plotted against γ . LO (red) and HO (blue). $\bar{\eta}_c = \eta_c \omega_r / K$. D: Power input output ratio. The set of parameter values: $1/\bar{\omega}_c=0.2$, $\omega_1=0.36$ in Eq. 16.

LO-driven cases

Here we assume that the OHC is primarily driven by the motion of LO rather than that of HO to examine if the amplitude gain can be larger. The meaning of this mode will be discussed later. It turns out that LO-driven modes are more effective than HO-driven modes.

viscous coupling

The amplitude gain for both LO and HO increases with the operating point variable γ (Fig. 9A). HO has somewhat higher peak frequency than LO for small γ (Fig. 9B). The phases of HO and O are both close to $\pi/4$ and HO tends to be ahead of LO except for where γ is small (Fig. 9C). The power amplification is not very large, similar to the amplitude of HO.

elastic coupling

An example is shown in Fig. 10. Another examine is shown in Appendix B. The amplitude gain can exceed 100 fold for the LO and 80 fold for HO (Fig. 10A). These values are somewhat less in Fig. B1A. The amplitude gain generally increases with the operating point variable γ as expected. This increase can be monotonic as in Fig. 10A. However, it can peak before γ reaches unity as shown in Fig. B1A in Appendix B, depending on the set of parameter values.

The peak frequencies are similar for both oscillators (Fig. 10B). The LO is ahead of HO in phase, indicating the amplifying role of the LO even though the difference is rather small (Fig. 10C). The effect of the LO in affecting the amplitude of LO is quite large despite its much smaller mass and stiffness. These features are shared by the plots in Appendix B.

The ratio of power output to input maximizes at a value of about 60 where the amplitude of HO is maximized (Fig. 10D).

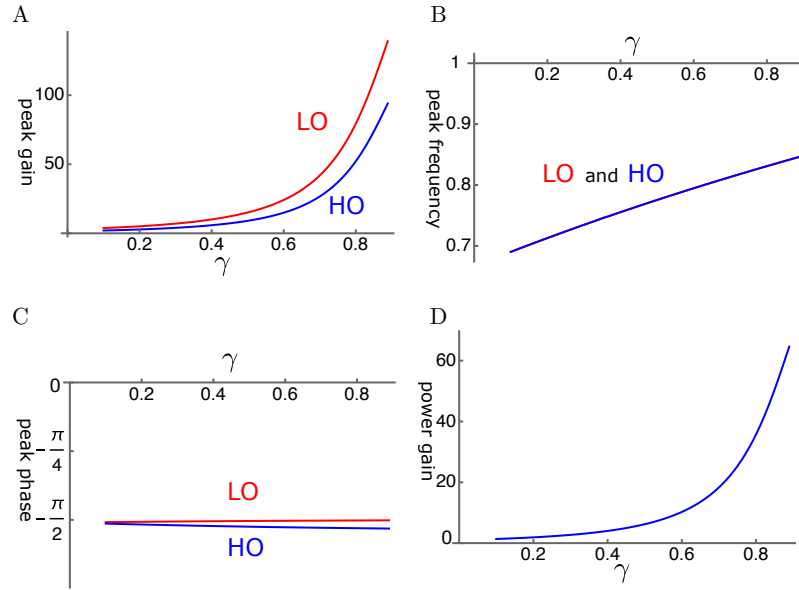


Figure 10: An example of LO-driven elastic coupled oscillators (LOE). A: Amplitude gain over SO mode, B: Peak frequency, and C: The phase with respect to the external force, of each oscillator, is plotted against γ . LO (red) and HO (blue). D: The ratio of power output to power input. The set of parameter values: $c=0.6$, $\omega_1=0.18$ in Eq. 17.

The frequency dependence shows quite sharp tuning together with the large amplitude gain (Fig. 11).

Comparison of the cases

With the constraint of the given values of the parameters, it is possible to observe the major difference in the four major cases. In addition, more generalized cases can be predicted by superposition of individual cases since our equations are linear.

The case of LO-stimulation with elastic coupling (LOE mode) is most effective in utilizing OHC. It leads to about 60 fold power gain (Fig. 10D) and amplitude gain of about 80 fold for HO (Fig. 10D). The case of HO-stimulation

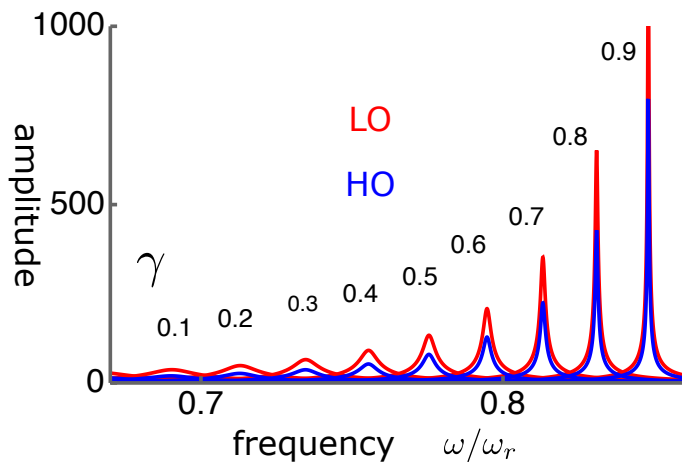


Figure 11: The amplitudes LO (red) and HO (blue) in LO-driven elastically coupled (LOE) oscillators. The abscissa is the frequency normalized to the resonance frequency ω/ω_r . The unit of the amplitude (ordinate axis) is f/K . The values of γ are from 0.1(left) to 0.9(right) with an increment of 0.1.

with elastic coupling (HOE mode) may lead to a relatively good amplitude gain for LO, even though it is less effective than LOE. In view of similar phase relationships of the oscillators in those two cases, a superposition of these two factors could be constructive.

Discussion

The examination presented here is more like a survey rather than a thorough analysis due to the relatively large number of parameters. In addition, the focus is on the high frequency performance. Nonetheless it is possible to observe general features of the models.

Input impedance mismatch

The coupled oscillator models can make OHCs more effective by reducing the constraint of impedance mismatch. However, the performance of coupled oscillator models significantly varies depending on the type of coupling and how OHCs are stimulated.

More specifically, optimal amplification of this system by the OHC is achieved in the case where coupling is elastic and the OHC is stimulated primarily by the oscillation of LO. Under such conditions, the gain is not impeded by a large stiffness mismatch between the OHC and the BM.

Some characteristics

Detailed properties of coupled oscillators vary depending on the set of parameter values. Under the conditions for larger amplifier gain, the following observations can be made.

Frequency dependence

Strong coupling is required for making OHCs effective. In the case of elastic coupling, for example, the stiffness of the coupling element must be similar to that of the elastic element of LO. This condition appears to lead to another feature that the resonance frequency of LO is somewhat lower than that of HO. With increased OHC electromotility (increased γ), the resonance frequency tends to increase, reminiscent of the half-octave shift [34, 35].

Stability and γ -dependence

Amplitude gain of a coupled oscillator is in general an increasing function of γ , the the activity of the motile element in the OHC. Some of the cases (See Fig. 10A) show monotonic increase with γ similar to the single mode oscillator with low elastic load (See Fig. 6A).

However, depending on the condition, it can peak before the operating point variable γ reaches unity (See Figs. 8A and B1A in Appendix B).

Although such a behavior is not intuitive, it is compatible with a report that lowering prestin density in OHCs by 34% does not have any reduction in the sensitivity of the ear [36]. That is because both A and B are proportional to N , the number of motile units in an OHC (See Table 1). Thus, N and γ have the same effect on these parameters.

Amplitude gains are very sensitive to parameter values. They can be a smooth function of the operating point variable γ as shown in the figures. They can show singular dependence on γ , indicating spontaneous oscillation. These properties could have bearing on otoacoustic emissions [37].

Structural implications

The behavior of the equations examined must have a structural basis, including the nature of coupling elements, the effect of cell length, and movements in the subtectorial space.

Nature of coupling

The cell body of OHCs is held by the reticular lamina at the apical end, forming tight junctions, and by Deiters' cup at the basal end. This structure introduces viscoelastic interaction with Deiters' cells [38]. Being held taut appears to indicate that OHCs are subjected to elastic load. However, Deiters' cap could provide viscous coupling [10, 27]. The present analysis shows such a mode is not very effective to enhance the amplitude of LO at high frequencies.

Cell length

Short hair cells are more effective in the amplifying role with larger amplifying parameter u because of their smaller C_0 and larger k_o . That is clearly illustrated

by guinea pigs, which show a large length gradient from the base ($20\ \mu\text{m}$) to the apex ($\sim 100\ \mu\text{m}$). However, mice show a much smaller gradient. The difference is only 1.5 times in length [39]. That indicates the significance of the structure of the organ of Corti in frequency tuning. Such a variability in cell length indicates the significance of the structural parameters and is thus compatible with the present analysis.

Subtectorial drag and OHC stimulation

The models examined in the present treatment assume that the main drag of the system is associated with HO. Without this assumption LO cannot influence the movement of HO. Such a condition could be realized if the main drag imposed on HO is outside the subtectorial gap.

However, the most likely source of the main drag of the system would be the shear in the subtectorial space between the tectorial membrane and the reticular lamina [40]. This picture indicates that the shear is associated with the motion of HO. If we accept that hair bundle bending is associated with this shear, the OHC should be stimulated by the displacement of HO. That leads to HO-stimulation models.

Can the hair bundle of the OHC be primarily stimulated by LO without incurring significant drag? Such a condition could be realized if LO moves the hair bundle in the direction perpendicular to the reticular lamina, resulting in effective bending of the hair bundle. However, the movement of LO should not incur significant drag. It would be possible that displaced water volume could be accommodated by local displacement of the TM owing to its pliability [41] and mechanical anisotropy [42, 43]. Then, the movement of LO does not result in viscous drag because it does not lead to fluid flow along the gap.

Speed of the motile element

We assumed that prestin, the motile protein that drives OHCs, undergoes conformational transitions fast enough so that mechanical constraints determine the frequency dependence. This assumption is consistent with the experimental data on isometric force generation by OHC [44] and current noise spectrum of OHC membrane [45]. It is also in line with a recent analysis that movement of organ of Corti measured with OCT is consistent with the cycle-by-cycle force application [46].

However, the frequency of conformational changes must have an upper bound. Recent reports that the roll-off frequencies of the voltage-dependent component of OHC membrane capacitance suggest 30 kHz, [47] higher than older values of up to 20 kHz [48, 49]. Those gating frequencies reported could reflect extracellular factors, such as viscoelastic process, of their experimental configuration.

The present study provides a new perspective: with a large gain obtained by coupled oscillators, this issue is not so important. With a finite gating

frequency ω_g , the amplitude is attenuated by a factor $1/(1 + \omega_g/\omega)$ [50]. If the gating frequency is 20 kHz, this attenuation factor is 1/3 at 40 kHz, a small fraction of the expected gain.

Implication to macroscopic models

A good number of macroscopic models of cochlear mechanics [4] assume that OHCs apply force directly on the basilar membrane (BM). Such models ignore issues resulting from microscopic structure, such as low-pass characteristics of intrinsic cellular electric circuit and impedance mismatch.

Paradoxically, the present analysis of coupled oscillator models shows a resemblance to the assumptions of those macroscopic models: The amplifier gain is not seriously constrained by the impedance mismatch. Both the amplitude and the phase of the two oscillators are not so large.

Conclusions

Large impedance mismatch between the BM and an OHC impedes energy transmission from the softer OHC to the oscillation of the stiffer BM if the BM and the OHC are in the same oscillator. However, if these elements are incorporated in separate oscillators that are coupled, a significant improvement in the efficiency of energy transmission can be achieved.

Among the modes of motion examined, the system of elastically coupled with LO-stimulated OHC is most effective in utilizing the OHC as the amplifier. Under optimal conditions, both amplitudes and phases of these oscillators are close because these oscillators are strongly coupled.

The models examined here are the simplest possible cases. The real ear would be much more complex and can have more modes of motion. Nonetheless, these simple model systems could provide some insight into the working of the real system. It is likely that multiple modes of motion supported by the complexity of the organ of Corti is essential for the performance of the mammalian ear by making OHCs effective as the amplifier.

Acknowledgments

I thank Drs. Richard Chadwick and Catherine Weisz of NIDCD for helpful comments and Drs. Matthew Kelley and Inna Belyantseva for reading the manuscript. This research was supported in part by the Intramural Research Program of the NIH, NIDCD.

References

1. Vater, M., and M. Kössl, 2011. Comparative aspects of cochlear functional organization in mammals. *Hearing Res.* 273:89–99.
2. Dallos, P., X. Wu, M. A. Cheatham, J. Gao, J. Zheng, C. T. Anderson, S. Jia, X. Wang, W. H. Y. Cheng, S. Sengupta, D. Z. Z. He, and J. Zuo, 2008. Prestin-based outer hair cell motility is necessary for mammalian cochlear amplification. *Neuron* 58:333–339.
3. Robles, L., and M. A. Ruggero, 2001. Mechanics of the mammalian cochlea. *Physiol Rev* 81:1305–1352.
4. de Boer, E., and A. Nuttall, 2010. Cochlear mechanics, tuning, nonlinearities. In P. A. Fuchs, editor, *The Oxford Handbook of Auditory Science volume 1: The Ear*, Oxford University Press, Oxford, UK, 139–177.
5. deBoer, E., 1980. Auditory physics. Physical principles in hearing theory. I. *Phys. Rep.* 62:87–174.
6. Kim, D. O., S. T. Neely, C. E. Molnar, and J. W. Matthews, 1980. An active cochlear model with negative damping in the partition: comparison with Rhode’s ante- and post-mortem observations. In G. van den Brink, and F. A. Bilsen, editors, *Psychological, physiological and behavioral studies of hearing*, Delft University Press, Delft, the Netherlands, 7–14.
7. Zweig, G., 1991. Finding the impedance of the organ of Corti. *J. Acoust. Soc. Am.* 89:1229–1254.
8. Neely, S. T., and D. O. Kim, 1986. A model for active elements in cochlear biomechanics. *J. Acoust. Soc. Am.* 79:1472–1480.
9. Chadwick, R., E. Dimitriadis, and K. Iwasa, 1996. Active control of waves in a cochlear model with subpartitions. *Proc. Natl. Acad. Sci. USA* 93:2564–2569.
10. Altoè, A., J. B. Dewey, K. K. Charaziak, J. S. Oghalai, and C. A. Shera, 2022. Overturning the mechanisms of cochlear amplification via area deformations of the organ of Corti. *J. Acoust. Soc. Am.* 152:2227– 2239.
11. Rabbitt, R., and T. Bidone, 2023. A parametric blueprint for optimum cochlear outer hair cell design. *J Roy Soc Interface* 20:20220762.
12. Mountain, D. C., and A. E. Hubbard, 1994. A piezoelectric model of outer hair cell function. *J. Acoust. Soc. Am.* 95:350–354.
13. Iwasa, K. H., 2017. Negative membrane capacitance of outer hair cells: electromechanical coupling near resonance. *Sci. Rep.* 7:12118.

14. Jawadi, Z., B. Applegate, and J. Oghalai, 2016. Optical Coherence Tomography to Measure Sound-Induced Motions Within the Mouse Organ of Corti In Vivo. *Methods. Mol. Biol.* 1427:449–462.
15. Cooper, N. P., A. Vavakou, and M. van der Heijden, 2018. Vibration hotspots reveal longitudinal funneling of sound-evoked motion in the mammalian cochlea. *Nature Commun* 9:3054.
16. Dong, W., A. Xia, P. Raphael, S. Puria, B. Applegate, and J. Oghalai, 2018. Organ of Corti vibration within the intact gerbil cochlea measured by volumetric optical coherence tomography and vibrometry. *J. Neurophysiol.* 120:2847–2857.
17. Frost, B., C. Strimbu, and E. Olson, 2022. Using volumetric optical coherence tomography to achieve spatially resolved organ of Corti vibration measurements. *J. Acoust. Soc. Am.* 151:1115.
18. He, W., G. Burwood, E. Porsov, A. Fridberger, A. Nuttall, and T. Ren, 2022. The reticular lamina and basilar membrane vibrations in the transverse direction in the basal turn of the living gerbil cochlea. *Sci. Rep.* 12:19810.
19. Iwasa, K. H., 2021. Kinetic membrane model of outer hair cells. *Biophys. J.* 120:122–132.
20. Zheng, J., W. Shen, D. Z.-Z. He, K. B. Long, L. D. Madison, and P. Dallos, 2000. Prestin is the motor protein of cochlear outer hair cells. *Nature* 405:149–155.
21. Morse, P. M., and K. U. Ingard, 1968. *Theoretical Acoustics*. Princeton University Press, Princeton, New Jersey.
22. Mercer, C. A., P. L. Rees, and F. J. Fahy, 1971. Energy flow between two weakly coupled oscillators subject to transient excitation. *J. Sound Vib.* 15:373–379.
23. Iwasa, K. H., and M. Adachi, 1997. Force generation in the outer hair cell of the cochlea. *Biophys. J.* 73:546–555.
24. Johnson, S. L., M. Beurg, W. Marcotti, and R. Fettiplace, 2011. Prestin-driven cochlear amplification is not limited by the outer hair cell membrane time constant. *Neuron* 70:1143–1154.
25. Nam, J.-H., A. W. Peng, and A. J. Ricci, 2015. Underestimated sensitivity of mammalian cochlear hair cells due to splay between stereociliary columns. *Biophys. J.* 108:2633–2647.
26. Russell, I. J., G. P. Richardson, and A. R. Cody, 1986. Mechanosensitivity of mammalian auditory hair cells *in vitro*. *Nature* 321:517–519.

27. Mammano, F., and R. Nobili, 1993. Biophysics of the cochlea: linear approximation. *J. Acoust. Soc. Am.* 93:3320–3332.
28. Greenwood, D. D., 1990. A cochlear frequency-position function for several species—29 years later. *J. Acoust. Soc. Am.* 87:2592–1605.
29. Olson, E. S., H. Duifhuis, and C. R. Steele, 2012. Von Békésy and cochlear mechanics. *Hearing Res.* 213:31–43.
30. Gummer, A. W., B. M. Johnstone, and N. J. Armstrong, 1981. Direct measurement of basilar membrane stiffness in the guinea pig. *J. Acoust. Soc. Am.* 70:1298–1309.
31. Miller, C. E., 1985. Structural implications of basilar membrane compliance measurements. *J. Acoust. Soc. Am.* 77:1465–1474.
32. Batchelor, G. K., 1967. An introduction to fluid dynamics. Cambridge University Press, Cambridge, UK.
33. Ospeck, M., X.-X. Dong, and K. H. Iwasa, 2003. Limiting frequency of the cochlear amplifier based on electromotility of outer hair cells. *Biophys. J.* 84:739–749.
34. Ruggero, M., N. Rich, A. Recio, S. Narayan, and L. Robles, 1997. Basilar-membrane responses to tones at the base of the chinchilla cochlea. *J. Acoust. Soc. Am.* 101:2151–2163.
35. Ramamoorthy S, N. A., 2012. Half-octave shift in mammalian hearing is an epiphenomenon of the cochlear amplifier. *PLoS One* 7:e45640.
36. Yamashita, T., J. Fang, J. Gao, Y. Yu, M. M. Lagarde, and J. Zuo, 2012. Normal hearing sensitivity at low-to-middle frequencies with 34% prestin-charge density. *PLoS One* 7:e45453.
37. Kemp, D., 2010. Otoacoustic emissions and evoked potentials. In P. A. Fuchs, editor, *The Oxford Handbook of Auditory Science volume 1: The Ear*, Oxford University Press, Oxford, UK, 93–137.
38. Zhou, W., T. Jabeen, S. Sabha, J. Becker, and J. Nam, 2022. Deiters Cells Act as Mechanical Equalizers for Outer Hair Cells. *J. Neurosci.* 42:8361–8372.
39. Zajic, G., and J. Schacht, 1987. Comparison of isolated outer hair cells from five mammalian species. *Hearing Res.* 26:249–256.
40. Allen, J., 1980. Cochlear micromechanics—A physical model of transduction. *J. Acoust. Soc. Am.* 68:1660–1670.

41. Teudt, I., and C. Richter, 2014. Basilar membrane and tectorial membrane stiffness in the CBA/CaJ mouse. *J. Assoc. Res. Otolaryngol.* 15:675–694.
42. Gavara, N., and R. Chadwick, 2009. Collagen-based mechanical anisotropy of the tectorial membrane: implications for inter-row coupling of outer hair cell bundles. *PLoS One* 4:e4877.
43. Masaki, K., J. Gu, R. Ghaffari, G. Chan, R. Smith, D. Freeman, and A. Aranyosi, 2009. Col11a2 deletion reveals the molecular basis for tectorial membrane mechanical anisotropy. *Biophys. J.* 96:4717–4724.
44. Frank, G., W. Hemmert, and A. W. Gummer, 1999. Limiting dynamics of high-frequency electromechanical transduction of outer hair cells. *Proc. Natl. Acad. Sci. USA* 96:4420–4425.
45. Dong, X., D. Ehrenstein, and K. H. Iwasa, 2000. Fluctuation of motor charge in the lateral membrane of the cochlear outer hair cell. *Biophys J* 79:1876–1882.
46. Dewey, J. B., A. Altoé, C. A. Shera, B. E. Applegate, and J. S. Oghalai, 2021. Cochlear outer hair cell electromotility enhances organ of Corti motion on a cycle-by-cycle basis at high frequencies in vivo. *Proc Natl Acad Sci USA* 118:e2025206118.
47. Santos-Sacchi J, N. D., Bai JP, 2023. Megahertz Sampling of Prestin (SLC26a5) Voltage-Sensor Charge Movements in Outer Hair Cell Membranes Reveals Ultrasonic Activity that May Support Electromotility and Cochlear Amplification. *J Neurosci.* 43:2460–2468.
48. Santos-Sacchi, J., and W. Tan, 2018. The Frequency Response of Outer Hair Cell Voltage-Dependent Motility Is Limited by Kinetics of Prestin. *J. Neurosci.* 38:5495–5506.
49. Santos-Sacchi, J., K. H. Iwasa, and W. Tan, 2019. Outer hair cell electromotility is low-pass filtered relative to the molecular conformational changes that produce nonlinear capacitance. *J Gen Physiol* 151:1369–1385.
50. Iwasa, K., 2024. Not so presto? Can outer hair cells be sluggish? *AIP Conf. Proc.* 3062:050002.

Appendix A Single oscillator with OHC

Here we consider a case, in which an OHC incorporated into a system with mechanical resonance as illustrated in Fig. A1. Described first is the case of electrical stimulation. Then the treatment is extended to mechanical stimulation. That is followed by a numerical examination similar to those examination of coupled oscillators that is presented in the main part.

Electrical stimulation

The description largely follows the one-dimensional model [13], rather than the more realistic cylindrical model [19] for simplicity.

Motile element

Let the motile element in the lateral membrane of the OHC have two states, the long state L and the short state S , and let P be the fraction of the motile element in state L . The natural length of the cell would be $X_0 + aNP$, where a is the contribution of a single motile element to the cell length accompanied by conformational change from S to L . The same conformational change transfers a charge q across the membrane. The number of the motile elements in the cell is N .

With an external elastic load k_e , the displacement X due to the motile unit is given by

$$X = aNP k_e / (k_o + k_e), \quad (\text{A1})$$

where k_o is the structural stiffness of the cell. In addition, assume that P_∞ at equilibrium follows the Boltzmann distribution

$$P_\infty / (1 - P_\infty) = \exp[-\beta(G_0 + qV + aF_o)] \quad (\text{A2})$$

where $\beta = 1/(k_B T)$ with Boltzmann's constant k_B and the temperature T . The constant term is represented by G_0 . The quantities V and F_o are, respectively, the membrane potential and force applied from the external elastic load, which is associated with axial displacement X of the cell. Since the stiffness of the external elastic load is k_e , $F_o = k_e X$.

Equation of motion

The equation of motion of the system that is illustrated in Fig. A1 can be expressed by

$$m d^2 X / dt^2 + \eta dX / dt = k_o (X_\infty - X), \quad (\text{A3})$$

where $X_\infty = aNP_\infty k_o / (k_o + K)$ is the displacement that corresponds to equilibrium, m is the mass, and η drag coefficient. The inertia term can be justified if the system is not far from equilibrium [19]. The difference between the current displacement X and equilibrium displacement X_∞ is the driving force. The equation of motion (A16) can be expressed using variable P

$$m d^2 P / dt^2 + \eta dP / dt = (k_o + k_e)(P_\infty - P). \quad (\text{A4})$$

The amplitude x of displacement is related to p with

$$x = aNp k_o / (k_o + k_e), \quad (\text{A5})$$

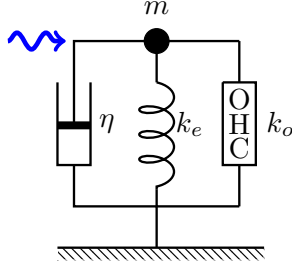


Figure A1: A simple system of OHC with mechanical load.

in the manner exactly corresponding to X and P , i.e. Eq. A1.

Now consider the response to a sinusoidal voltage waveform of small amplitude v and angular frequency ω . Let p the corresponding small amplitude of P .

$$V = V_0 + v \exp[i\omega t], \quad P = P_0 + p \exp[i\omega t].$$

Then the equation of motion (A10) is transformed into

$$p = \frac{-\beta\gamma q/4}{-\bar{\omega}^2 + i\bar{\omega}/\bar{\omega}_\eta + 1 + u_a k_e/(k_o + k_e)} v, \quad (\text{A6})$$

where $\bar{\omega}(= \omega/\omega_r)$ is the frequency normalized to the mechanical resonance frequency $\omega_r = \sqrt{(k_o + k_e)/m}$, $\bar{\omega}_\eta$ is normalized viscoelastic roll-off frequency, $\gamma = 4P_0(1 - P_0)$, and

$$u_a = \beta\gamma a^2 k_o N/4. \quad (\text{A7})$$

The coefficients γ and α originate from the expansion of the exponential term of P_∞ .

Response to hair bundle stimulation

The effect of hair bundle resistance R_a on the membrane potential V can be expressed

$$(e_{ec} - V)/R_a = (V - e_K)/R_m + C_0 dV/dt - Nq dP/dt, \quad (\text{A8})$$

where e_{ec} is the endocochlear potential, e_K is the resting potential of OHC, which is primarily determined by K^+ conductance, and R_a hair bundle conductance.

If we assume that stimulation at the hair bundle is periodic with angular frequency ω , introducing the time independent component R_0 and the relative amplitude \hat{r} of the hair bundle resistance R_a , we obtain

$$-i_0 \hat{r} = (\sigma + i\omega C_0)v - i\omega Nqp. \quad (\text{A9})$$

Here $i_0 = (e_{ec} - e_K)/(R_0 + R_m)$ is the steady state current and $\sigma = 1/R_0 + 1/R_m$ the steady state conductance, which can be dropped for high frequency stimulation because it is smaller than ωC_0 .

From the transformed equation of motion Eq. A6 and equation for receptor potential Eq. A9, p can be expressed as a linear function of r .

$$p(-\bar{\omega}^2 + i\bar{\omega}/\bar{\omega}_\eta + 1 + B) = i\frac{\beta\gamma i_0 q}{\omega C_0} \hat{r}, \quad (\text{A10})$$

with

$$B = u_a k / (k_o + k_e) + u_q, \quad \text{and} \quad (\text{A11})$$

$$u_q = \beta\gamma N q^2 / (4C_0), \quad (\text{A12})$$

which is the ratio of prestin capacitance at the zero-frequency limit to the structural capacitance. (appears in both 2017 paper and 2021 paper.) The equation shows that the damping term $1/\bar{\omega}_\eta = \omega_r/\omega_\eta$ must be small not to be overdamped. Notice also that $|p|$ is inversely proportional to C_0 .

Eq. A10, which is described by the variable p , can be rewritten by using x as

$$x(-\bar{\omega}^2 + i\bar{\omega}/\bar{\omega}_\eta + 1 + \gamma B) = i\frac{\gamma A}{\bar{\omega}} \hat{r}, \quad (\text{A13})$$

where A is defined by

$$A = \frac{i_o u}{\omega_r} \frac{k_o}{k_o + k_e} \quad \text{with} \quad (\text{A14})$$

$$u = \beta\gamma a q N / (4C_0). \quad (\text{A15})$$

Notice that Eqs. A15, A7, and A12 are, respectively, definitions of u , u_a , and u_q , which appear in the main text.

Mechanical stimulation

The equation of motion in the presence of an external force F is given by

$$m d^2 X / dt^2 + \eta dX / dt = k_o (X_\infty - X) + F. \quad (\text{A16})$$

By following the same transformation as performed on voltage driven equation, this equation can be transformed into

$$[-\bar{\omega}^2 + i(\bar{\omega}/\bar{\omega}_\eta - g\gamma A/\bar{\omega}) + 1 + \gamma B]x = \hat{f}, \quad (\text{A17})$$

if the change in the hair bundle resistance \hat{r} can be expressed gx and $\hat{f} = f/(k + k_o)$. This equation is exactly Eq. 8 in the main text.

Appendix B LOE another example

For LO-driven elastic coupled oscillators, peak gain increases with γ while γ is small. However, it may have a maximum before γ reaches unity, depending on parameter sets. An example is shown below.

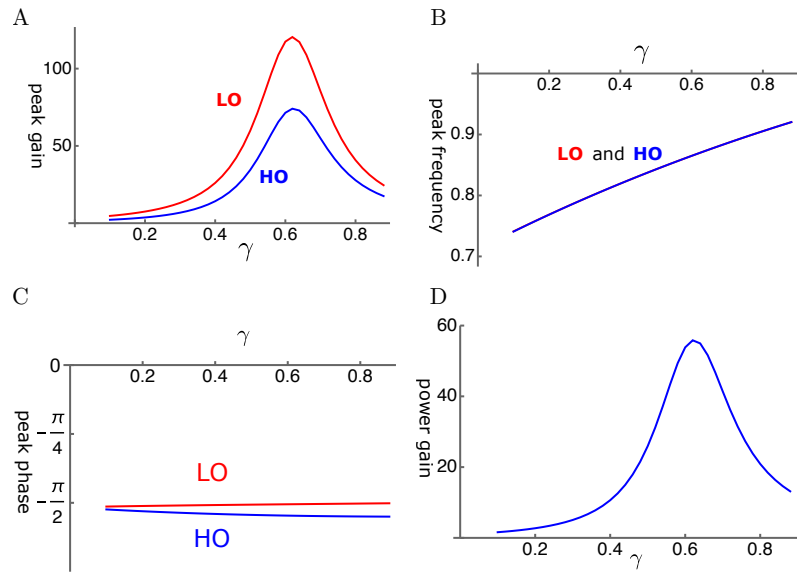


Figure B1: Another example of LO-driven elastic coupled oscillators (LOE). A: Amplitude gain over SO mode, B: Peak frequency, and C: The phase with respect to the external force, of each oscillator are plotted against γ . LO (red) and HO (blue). D: The ratio of power output to power input. The set of parameter values: $c=0.4$, $\omega_1=0.24$ in Eq. 17.